Modeling and control of a hybrid-fed Triple-Active Bridge converter

Rebecca Tarraf, David Frey, Sylvain Leirens, Sébastien Carcouet, Xavier Maynard, Yves Lembeye

energies

MDPI

Article

Modeling and Control of a Hybrid-Fed Triple-Active Bridge Converter

Rebecca Tarraf [1,*], David Frey [2], Sylvain Leirens [1], Sebastien Carcouet [1], Xavier Maynard [3] and Yves Lembeye [2]

[1] CEA, Leti, Université Grenoble Alpes, F-38000 Grenoble, France; sylvain.leirens@cea.fr (S.L.); sebastien.carcouet@cea.fr (S.C.)
[2] G2Elab, CNRS, Université Grenoble Alpes, F-38000 Grenoble, France; david.frey@g2elab.grenoble-inp.fr (D.F.); yves.lembeye@g2elab.grenoble-inp.fr (Y.L.)
[3] CEA, Liten, Université Grenoble Alpes, F-38000 Grenoble, France; xavier.maynard@cea.fr
* Correspondence: rebecca.tarraf@cea.fr

Abstract: In general, the structures of Multi-Active Bridge (MAB) converters that can be found in the literature are usually based on voltage converters. However, in some cases, it could be interesting to have a current-fed input due to load characteristics or operation constraints. This leads to a hybrid MAB structure mixing both current-fed and voltage-fed bridges. In this paper, a new hybrid-fed, fully coupled Triple-Active Bridge (TAB) converter topology with two voltage-fed ports and one current-fed port is studied, modelled and controlled. In the first place, a generalized average model (GAM) is developed for this system. After that, a reduced-order model is elaborated in order to simplify the behavioral study and control of this coupled system. A control strategy was also proposed in this paper, based on the developed mathematical model. Simulation results using Matlab/Simulink are presented to validate this study.

Keywords: Multi-Active Bridge (MAB) converter; current-fed converters; generalized average model; reduced-order model; control

Citation: Tarraf, R.; Frey, D.; Leirens, S.; Carcouet, S.; Maynard, X.; Lembeye, Y. Modeling and Control of a Hybrid-Fed Triple-Active Bridge Converter. *Energies* **2023**, *16*, 6007. https://doi.org/10.3390/en16166007

Academic Editors: Giuseppe Buja, Guidong Zhang, Gong Zheng, Xiangke Li, Minghao Wang, Shuo Yan and Qingsong Wang

Received: 21 July 2023
Revised: 9 August 2023
Accepted: 13 August 2023
Published: 16 August 2023

1. Introduction

Energy Hubs are a promising solution for the integration of renewable energy sources and the implementation of a decentralized energy system [1–3]. One interesting Energy Hub topology is the Multi-Active Bridge (MAB) converter, which appeared in recent years. It is the extension of the well-known Dual-Active Bridge (DAB) bidirectional DC-DC converter [4–6]. A MAB converter usually connects different energy sources, usually renewables (photovoltaic panels, wind turbines), loads and energy storage systems (ESS) together through a high frequency (HF) transformer, offering a full galvanic isolation between these ports. Energy storage is required in order to reduce the stress caused by intermittent energy sources. Batteries are very commonly used for this purpose.

Generally, studied MAB structures are based on voltage converters [7–12]. However, it can be interesting to have a current-fed port for some applications like connecting a PV panel or a battery system. Current-fed DAB converters have been presented in some previous papers [13–16]. Similarly, some previous works have introduced different topologies of multiport converters with one or more current-fed ports [17–19]. In [20], a new topology of a fully isolated, hybrid-fed TAB converter with full bridges on all its ports was presented, modelled and controlled. However, the three ports of the proposed structure were decoupled using a hardware decoupling method in order to simplify its control [21]. This will make the TAB converter act like two independent DAB converters from a control point of view. In other words, the decoupling of the ports transforms this Multi-Input Multi-Output (MIMO) system into two independent Single-Input Single-

Output (SISO) systems. Nevertheless, if the master port is lost in this case, the proposed control strategy will no longer be valid as the system will no longer be decoupled, and the two considered SISO systems will no longer be independent.

In this article, a generic model and control strategy are developed for the same topology presented in [20], but with fully coupled ports. The coupling between the ports is due to the presence of inductances at the transformer windings of all the ports. This will make this study generic and all-inclusive. Therefore, any simplification of the system, such as the nonexistence of an inductance at one of the ports for decoupling purposes (as presented in [20]), will be a particular case of the study presented in this article. Therefore, the proposed control strategy is more robust as it will remain valid even if one of the voltage-fed ports is lost.

Adding a current-fed port presents several advantages compared to classical voltage-fed converters, such as soft switching on the full operation range (even at light loads and when voltage mismatches occur) and the absence of an input capacitor on the current port, which can decrease the system's efficiency. The main drawback that the current-fed port introduces into the system is the complexity of its control. In fact, using a current inverter at one of the ports of a MAB converter imposes control conditions on all the system's ports. The non-compliance of one of these conditions can lead to many problems that can go from hard switching on some ports to brutal overvoltages on the current port.

The main purpose of this work is to study the feasibility of developing a closed-loop control strategy for the proposed fully coupled hybrid-fed MAB converter topology, considering the strict control restrictions imposed by the current-fed port that limit the operational area of this converter.

The mathematical modeling of a system makes the study of its dynamic behavior easier as it gives valuable insights into its operation and stability margins. In addition to that, it helps with the controller design. A generalized average model of a voltage-fed TAB converter was presented in [22].

In this paper, a topology of a fully coupled hybrid-fed TAB converter consisting of one current-fed port and two voltage-fed ports is studied and its control boundaries are explained. A generalized average model of this system is developed in order to calculate the control parameters of the system, and lead it approximately to a desired operating point. A controller then cancels the steady state error of the generalized average model, which is due to some simplifying assumptions that were made. A reduced-order model is also elaborated to simplify the study of the dynamic behavior and the design of the system's controllers. This will allow a real-time calculation of these controllers when the operating point or the control characteristics change. Finally, based on these developed mathematical models, a control strategy is proposed in order to regulate the power flows of this system while taking into consideration its control restrictions and imposing response characteristics such as time responses. Simulation results using the Matlab/Simulink platform and discussions are represented in Section 7 of this paper to validate this study and prove its feasibility.

2. The Proposed Converter

2.1. Topology of the Hybrid-Fed TAB Converter

A current inverter is a DC-AC converter where the DC side is a current source [23]. Figure 1 shows a topology of a coupled TAB converter having a current inverter connected to a temporary current source at port 1 and classical H-bridges at ports 2 and 3. Port 1 represents a unidirectional power source (ex., PV module), port 2 is bidirectional (ex., battery system, grid …) and port 3 is a DC load.

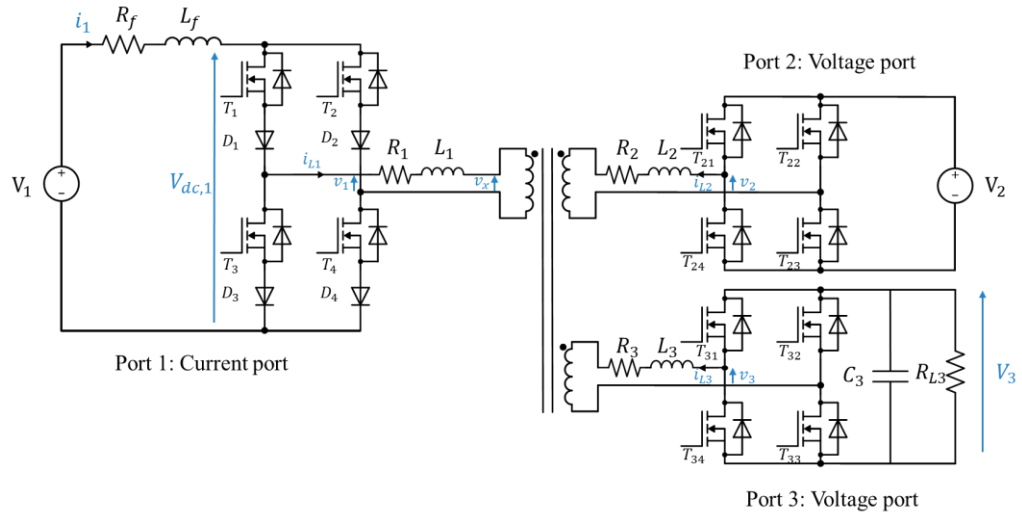

Figure 1. Coupled hybrid-fed TAB converter topology.

The ports of this TAB converter are coupled due to the presence of an inductance at each port, which can either be the leakage inductance of the transformer alone or in series with an externally connected one. Consequently, this converter behaves as a multivariable system having multiple inputs and outputs (MIMO). In other words, changing one control input parameter would affect all the converter's ports.

Controlling the power flows of this converter can be performed by regulating port 1's input current i_1 and port 3's output voltage V_3. Since the system is a coupled multiport converter, the algebraic sum of all input and output powers of the system would approximately be equal to zero (or equal to the system's losses). Therefore, the power that will be flowing from or into port 2 will be imposed by the following expression (neglecting the losses and the power stored in the magnetic core of the transformer):

$$P_2 = -P_1 - P_3,$$

where P_1 and P_3 are the powers flowing from or into ports 1 and 3, respectively.

The waveforms of this TAB's AC signals circulating in the transformer windings are shown in Figure 2, along with the command signals of switches T_1, T_{21} and T_{31}.

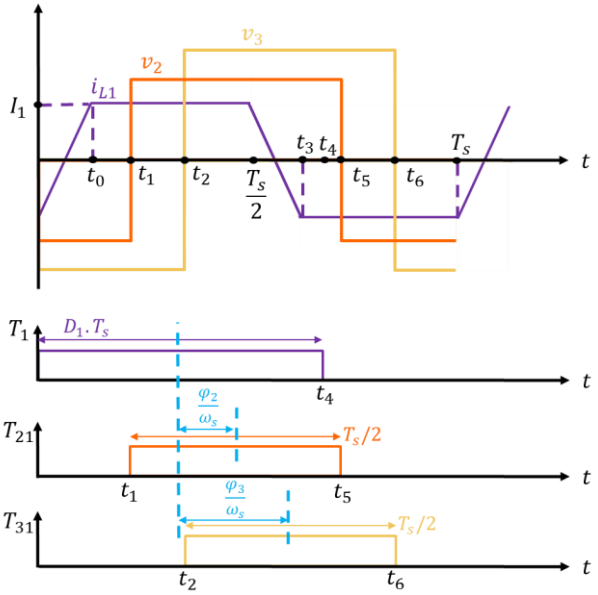

Figure 2. AC waveforms of the hybrid-fed TAB converter.

The trapezoidal current i_{L1} shown in Figure 2 is, as presented in Figure 1, the current circulating in the transformer winding at port 1. Parameters v_2 and v_3 are the AC voltages on the transformer side of ports 2 and 3, respectively. D_1 is the duty cycle of the command of port 1's switches ($0.5 < D_1 < 1$). φ_2 and φ_3 are the phase shifts (in radians) of the command signals of switches T_{21} and T_{31} with respect to T_1, respectively. The command duty cycles of the voltage ports' switches are fixed to $D_2 = D_3 = 50\%$ on all operation ranges, so v_2 and v_3 are two-leve—voltages, as shown in Figure 2. T_s is the switching period (f_s is the switching frequency).

The waveform shapes of Figure 2 are an approximation of the real signals' shapes. In reality, the current i_{L1} is not perfectly trapezoidal, as it is slightly affected by the switching of the voltage ports at instants t_1 and t_5 for port 2 on one hand and t_2 and t_6 for port 3 on the other hand.

Figure 3 shows the star-delta equivalent circuits of the transformer windings referred to port 1, with $v_2' = \frac{n_1}{n_2} \cdot S_2 \cdot$ and $v_3' = \frac{n_1}{n_3} \cdot S_3 \cdot V_3$. S_2 and S_3 are the switching functions of ports 2 and 3, respectively. n_i is the number of turns of the transformer winding of port #i. In these equivalent circuits, the current port 1 is replaced by an equivalent voltage source. The expression of v_1, the AC voltage on the transformer side of port 1, will be developed in Section 2.2. The voltage at the star point v_x can be obtained by the following expression:

$$v_x = L_a \cdot v_1 + L_b \cdot v_2' + L_c \cdot v_3', \tag{1}$$

where:

$$L_a = \frac{\frac{1}{\frac{1}{L_2'} + \frac{1}{L_3'}}}{L_1 + \frac{1}{\frac{1}{L_2'} + \frac{1}{L_3'}}}\ ;\ L_b = \frac{\frac{1}{\frac{1}{L_1} + \frac{1}{L_3'}}}{L_2' + \frac{1}{\frac{1}{L_1} + \frac{1}{L_3'}}}\ ;\ L_c = \frac{\frac{1}{\frac{1}{L_1} + \frac{1}{L_2'}}}{L_3' + \frac{1}{\frac{1}{L_1} + \frac{1}{L_2'}}}$$

with $L_k' = \left(\frac{n_1}{n_k}\right)^2 L_k$.

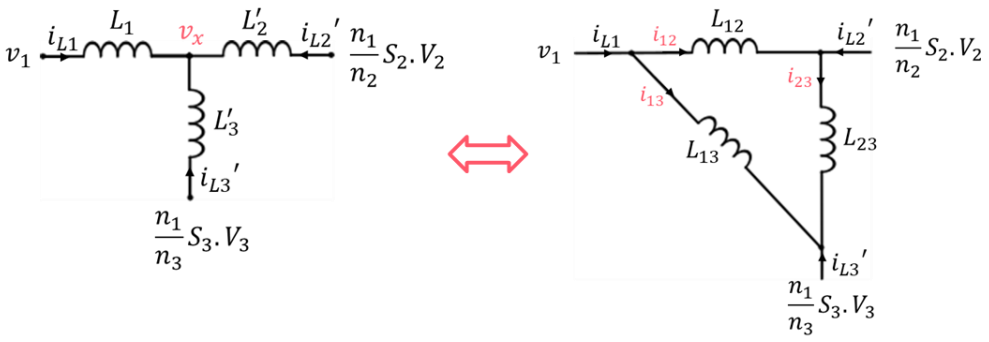

Figure 3. Star-delta transformation of the transformer windings referred to port 1.

The link inductances of the delta equivalent circuit are calculated as follows [21]:

$$L_{ij} = \begin{cases} NA, & \forall i = j \\ L_i' + L_j' + L_i' L_j' \left(\sum_{k \neq i,j}^{n} \frac{1}{L_k'} \right), & \forall i \neq j \end{cases}$$

2.2. Working Principle

At a certain operating point, the operation cycle of this TAB converter is divided into the following time intervals (Figure 2):

- $0 \le t \le t_0$:

At $t = 0$, switches T_1 and T_4 are turned on. T_2 and T_3 were already ON right before $t = 0$ from the previous cycle. In this time interval, all the switches of current port 1 are ON, meaning that $v_1 = 0$ (Figure 4a). Therefore, we can deduce from expression (1) that $v_x = L_b . v_2' + L_c \cdot v_3'$. At the voltage ports, T_{22}, T_{24}, T_{32} and T_{34} should be ON, so that $v_2' = -V_2 \cdot \frac{n_1}{n_2}$, $v_3' = -V_3 \cdot \frac{n_1}{n_3}$ and $v_x < 0$. This will allow the transformer current i_{L1} of port 1 to increase from $-I_1$ to I_1 in this interval. i_{L1} is represented by the following expression (neglecting the series resistance R_1 of the leakage inductance at port 1):

$$i_{L1}(t) = -\frac{v_x}{L_1} t - I_1 = \frac{L_b \cdot V_2 \cdot \frac{n_1}{n_2} + L_c \cdot V_3 \cdot \frac{n_1}{n_3}}{L_1} t - I_1, \quad (2)$$

where I_1 is the value of the input current i_1 of the current port at the chosen operating point. This current is considered constant at each operating point as it is limited by the input inductance L_f, of which the value is a lot bigger than the value of the leakage inductance L_1.

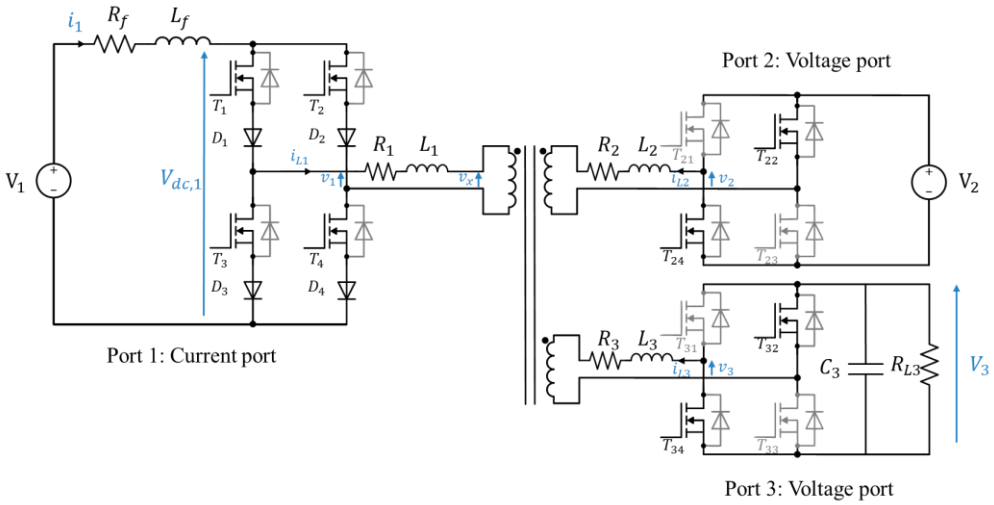

(**a**)

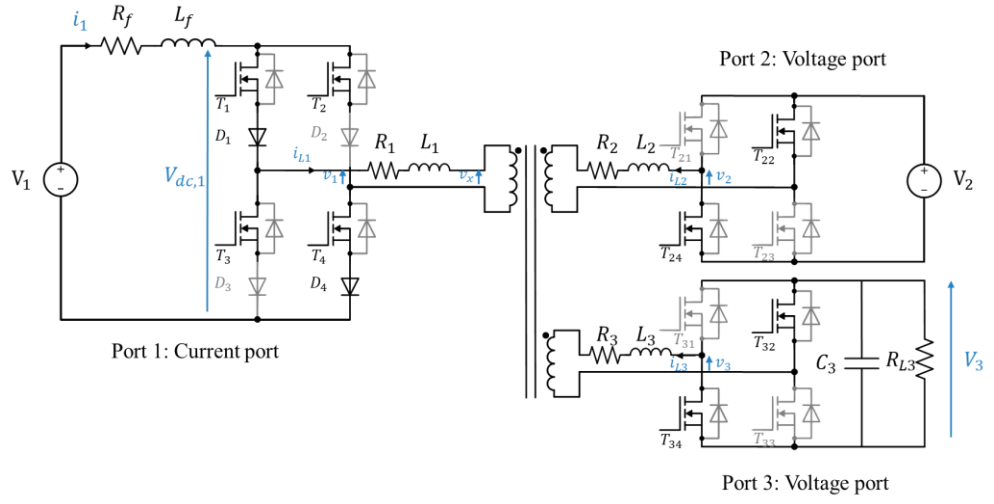

(**b**)

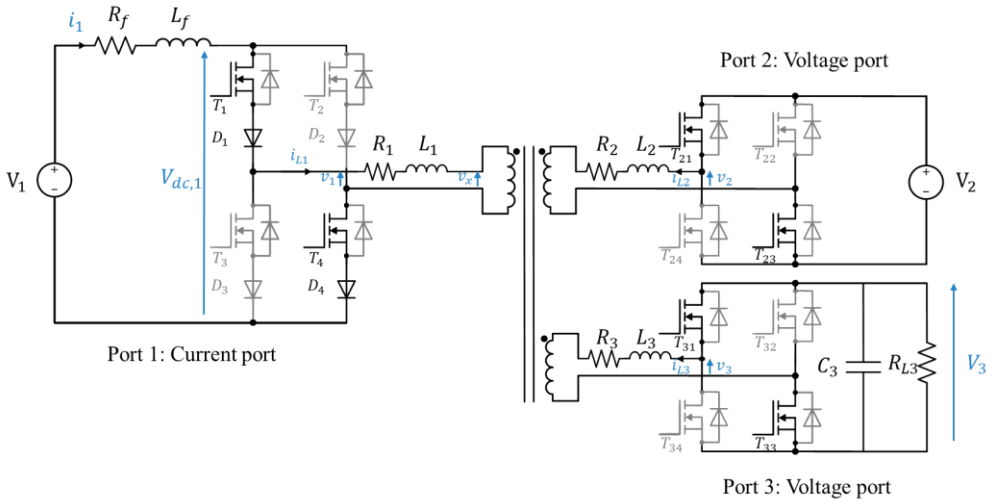

(**c**)

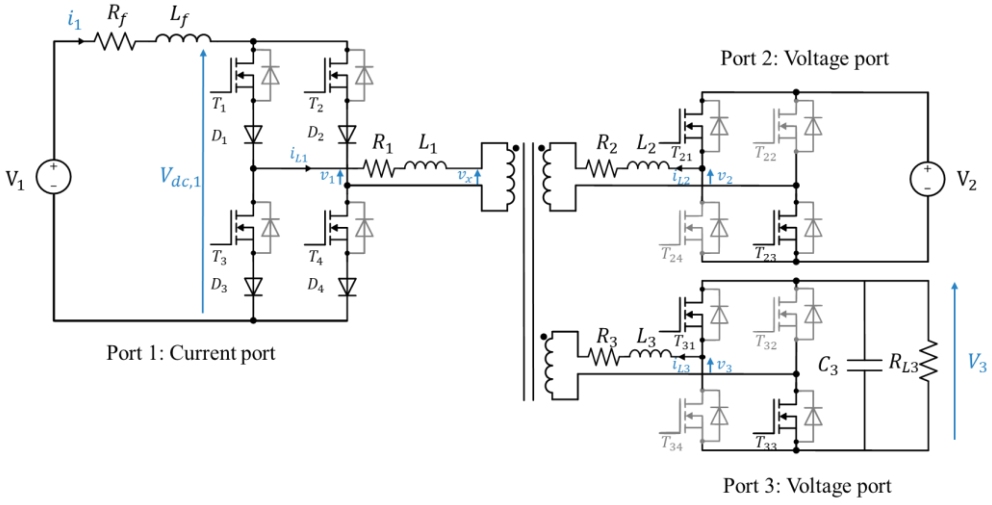

(**d**)

Figure 4. Equivalent circuits of the converter at: (**a**) $0 < t < t_0$; (**b**) $t_0 < t < t_1$; (**c**) $t_2 < t < \frac{T_s}{2}$; (**d**) $\frac{T_s}{2} < t < t_3$ (switches in grey are OFF).

As i_{L1} gets closer to I_1, the current starts passing more through the diodes D_1 and D_4 and less through D_2 and D_3. At $t = t_0$, the diodes D_2 and D_3 are naturally turned off (Figure 4b).

- $t_0 \leq t \leq \frac{T_s}{2}$:

In this time interval, the input current I_1 passes through T_1, T_4, D_1 and D_4 and $i_{L1} = I_1$. Switches T_2 and T_3 can be turned off between t_0 and t_1 at zero current (ZCS). The switching of the voltage ports is then achieved in order to allow the transformer current i_{L1} to switch in the next time interval. At $t = t_1$, voltage port 2's H-bridge is switched and $v_2{}' = V_2 \cdot \frac{n_1}{n_2}$. At $t = t_2$, voltage port 3's H-bridge is switched and $v_3{}' = V_3 \cdot \frac{n_1}{n_3}$ (Figure 4c). Ideally, this does not affect the transformer's current value i_{L1} since it is imposed by the current source ($L_f \gg L_1$). However, in a real application, this current is slightly affected. In this model, the ideal case is considered. Consequently, this approximation of a perfectly trapezoidal current i_{L1} and the neglect of the series resistance R_1 leads to the following expression of the AC voltage at port 1:

$$v_1 = v_x = \frac{L_b \cdot v_2{}' + L_c \cdot v_3{}'}{(1 - L_a)} > 0$$

- $\frac{T_s}{2} \leq t \leq t_3$:

At $t = \frac{T_s}{2}$, T_2 and T_3 are turned on at zero current. Therefore, all the current inverter's switches are ON again and the voltage $v_1 = 0$ (Figure 4d). The star point voltage will be $v_x = L_b.v_2' + L_c.v_3' > 0$, with $v_2' = V_2 \cdot \frac{n_1}{n_2}$ and $v_3' = V_3 \cdot \frac{n_1}{n_3}$. The transformer current at port 1 decreases from I_1 to $-I_1$ and it is represented by the following expression:

$$i_{L1}(t) = \frac{-v_x}{L_1}\left(t - \frac{T_s}{2}\right) + I_1 = -\frac{\left(L_b \cdot V_2 \cdot \frac{n_1}{n_2} + L_c \cdot V_3 \cdot \frac{n_1}{n_3}\right)}{L_1}\left(t - \frac{T_s}{2}\right) + I_1 \quad (3)$$

At $t = t_3$, D_1 and D_4 are naturally blocked.

- $t_3 \leq t \leq T_s$:

The input current passes entirely through T_2, T_3, D_2 and D_3 in this time interval and $i_{L1} = -I_1$. At $t = t_4$, T_1 and T_4 are turned off at zero current. At $t = t_5$ and $t = t_6$, voltage ports 2 and 3 are switched, respectively, and $v_2' = -V_2 \cdot \frac{n_1}{n_2}$, $v_3' = -V_3 \cdot \frac{n_1}{n_3}$. The AC voltage at port 1 will be:

$$v_1 = v_x = \frac{L_b \cdot v_2' + L_c \cdot v_3'}{(1 - L_a)} < 0$$

This cycle is then repeated for each switching period T_s.

3. Operating Conditions

In order to be able to transfer power between ports with soft switching on the whole operation range for all the active bridges while avoiding overvoltage at port 1, three main conditions should be respected:

(a) To avoid overvoltage and have a soft switching at port 1, the switches of the current inverter should not be turned off before the complete reversal of the transformer current i_{L1} and the blocking of their series diodes. Otherwise, these switches would block an important current in the link inductance, which will cause brutal overvoltage at port 1. This condition can be written as follows:

$$t_4 \geq t_3 \rightarrow D_1 T_s \geq \frac{T_s}{2} + t_0$$

With $t_0 = \frac{2L_1 I_1}{\left(L_b \cdot V_2 \cdot \frac{n_1}{n_2} + L_c \cdot V_3 \cdot \frac{n_1}{n_3}\right)}$ from Equation (2).

Therefore,

$$D_1 \geq \frac{2L_1 I_1}{\left(L_b \cdot V_2 \cdot \frac{n_1}{n_2} + L_c \cdot V_3 \cdot \frac{n_1}{n_3}\right) \cdot T_s} + \frac{1}{2} \quad (4)$$

(b) The voltage ports' AC voltages v_2' and v_3' should be reversed after the current i_{L1}'s full reversal and the blocking of both the diodes and their series switches at port 1. If v_2 and/or v_3 are reversed before that, the current i_{L1} may not be able to reverse, so no power can be exchanged between the ports. Additionally, if they are reversed between the blocking of the diodes and their series switches, the diodes can be turned on again, causing overvoltage at port 1. This condition also ensures a soft switching at the voltage ports and it can be written as the two following expressions:

$$t_5 \geq t_4 \rightarrow \frac{D_1 T_s}{2} + \varphi_2 \frac{T_s}{2\pi} + \frac{T_s}{4} \geq D_1 T_s$$

$$t_6 \geq t_4 \rightarrow \frac{D_1 T_s}{2} + \varphi_3 \frac{T_s}{2\pi} + \frac{T_s}{4} \geq D_1 T_s$$

Therefore,

$$\varphi_2 \geq \pi \cdot \left(D_1 - \frac{1}{2}\right) \tag{5}$$

$$\varphi_3 \geq \pi \cdot \left(D_1 - \frac{1}{2}\right) \tag{6}$$

We can deduce from Equations (2) and (3) that the slope of current i_{L1} during its reversal is proportional to $-v_x = -(L_b \cdot v_2' + L_c \cdot v_3')$. Therefore, the reversal of this current is guaranteed if both AC voltages of ports 2 and 3 have the same sign (both negative for a positive slope or both positive for a negative slope). Additionally, current i_{L1}'s slope will be maximized this way. Consequently, conditions (5) and (6) should always be respected simultaneously.

As we can notice, conditions (4) to (6) depend on the operating point of the converter as I_1, V_3, D_1, φ_2 and φ_3 vary according to the desired power flows, making the control of this topology complex.

4. Full-Order Generalized Average Model of the Hybrid-Fed TAB Converter

The state space equations of the studied system are:

- $L_f \frac{di_1}{dt} = V_1 - V_{dc,1} - R_f \cdot i_1$
- $C_3 \frac{dV_3}{dt} = -\frac{V_3}{R_{L3}} + S_3 \cdot i_{13} \cdot \frac{n_1}{n_3} + S_3 \cdot i_{23} \cdot \frac{n_1}{n_3}$
- $L_{12} \frac{di_{12}}{dt} = v_1 - \frac{n_1}{n_2} S_2 \cdot V_2 - R_{12} \cdot i_{12}$
- $L_{13} \frac{di_{13}}{dt} = v_1 - \frac{n_1}{n_3} S_3 \cdot V_3 - R_{13} \cdot i_{13}$

$$L_{23} \frac{di_{23}}{dt} = \frac{n_1}{n_2} S_2 \cdot V_2 - \frac{n_1}{n_3} S_3 \cdot V_3 - R_{23} \cdot i_{23}\,, \tag{7}$$

with:

$$V_{dc,1} = \begin{cases} v_1 & for\ 0 \leq t \leq \frac{T_s}{2} \\ -v_1 & for\ \frac{T_s}{2} \leq t \leq T_s \end{cases};$$

$$S_2(t) = \begin{cases} 1\ for & t_1 \leq t < t_5 \\ -1\ for & 0 \leq t < t_1\ and\ t_5 \leq t < T_s \end{cases};$$

$$S_3(t) = \begin{cases} 1\ for & t_2 \leq t < t_6 \\ -1\ for & 0 \leq t < t_2\ and\ t_6 \leq t < T_s \end{cases}.$$

The conventional average modelling usually used for power electronic converters takes into consideration the average values of the state variables in order to transform this discontinuous time model into a continuous one. This averaging method cannot be implemented for a TAB converter as it results in zero transformer current (since it is an AC variable). Therefore, the generalized average model of this system is developed in order to study it as a continuous time model while representing its AC signals with more precision than the classical average model. Therefore, DC signals will be represented by their average values (0th Fourier series coefficient) and AC signals will be represented by their fundamentals (1st Fourier series coefficient) [24].

The kth coefficient of the Fourier series of a variable x is denoted as $\langle x \rangle_k$, and it is a complex number:

$$\langle x \rangle_k = \langle x \rangle_{kR} + j\langle x \rangle_{kI} \tag{8}$$

R and I refer to the real and imaginary parts of the complex number. The large signal model of the system is derived from (7) as:

$$
\begin{aligned}
&\frac{d\langle i_1\rangle_0}{dt} = \frac{V_1}{L_\mathrm{f}} - \frac{\langle V_{dc,1}\rangle_0}{L_\mathrm{f}} - \frac{R_\mathrm{f}}{L_\mathrm{f}} \cdot \langle i_1\rangle_0 \\
&\frac{d\langle V_3\rangle_0}{dt} = -\frac{\langle V_3\rangle_0}{C_3 R_{L3}} + \frac{2}{C_3} \cdot \frac{n_1}{n_3} \cdot \langle S_3\rangle_{1R} \cdot \langle i_{13}\rangle_{1R} + \frac{2}{C_3} \cdot \frac{n_1}{n_3} \cdot \langle S_3\rangle_{1I} \cdot \langle i_{13}\rangle_{1I} + \frac{2}{C_3} \cdot \frac{n_1}{n_3} \cdot \langle S_3\rangle_{1R} \cdot \langle i_{23}\rangle_{1R} \\
&\qquad + \frac{2}{C_3} \cdot \frac{n_1}{n_3} \cdot \langle S_3\rangle_{1I} \cdot \langle i_{23}\rangle_{1I} \\
&\frac{d\langle i_{12}\rangle_{1R}}{dt} = -\frac{R_{12}}{L_{12}} \cdot \langle i_{12}\rangle_{1R} + \omega_s \cdot \langle i_{12}\rangle_{1I} + \frac{\langle v_1\rangle_{1R}}{L_{12}} - \frac{n_1}{n_2}\frac{\langle S_2\rangle_{1R}}{L_{12}} \cdot V_2 \\
&\frac{d\langle i_{12}\rangle_{1I}}{dt} = -\omega_s \cdot \langle i_{12}\rangle_{1R} - \frac{R_{12}}{L_{12}} \cdot \langle i_{12}\rangle_{1I} + \frac{\langle v_1\rangle_{1I}}{L_{12}} - \frac{n_1}{n_2}\frac{\langle S_2\rangle_{1I}}{L_{12}} \cdot V_2 \\
&\frac{d\langle i_{13}\rangle_{1R}}{dt} = -\frac{R_{13}}{L_{13}} \cdot \langle i_{13}\rangle_{1R} + \omega_s \cdot \langle i_{13}\rangle_{1I} + \frac{\langle v_1\rangle_{1R}}{L_{13}} - \frac{n_1}{n_3}\frac{\langle S_3\rangle_{1R}}{L_{13}} \cdot \langle V_3\rangle_0 \\
&\frac{d\langle i_{13}\rangle_{1I}}{dt} = -\omega_s \cdot \langle i_{13}\rangle_{1R} - \frac{R_{13}}{L_{13}} \cdot \langle i_{13}\rangle_{1I} + \frac{\langle v_1\rangle_{1I}}{L_{13}} - \frac{n_1}{n_3}\frac{\langle S_3\rangle_{1I}}{L_{13}} \cdot \langle V_3\rangle_0 \\
&\frac{d\langle i_{23}\rangle_{1R}}{dt} = -\frac{R_{23}}{L_{23}} \cdot \langle i_{23}\rangle_{1R} + \omega_s \cdot \langle i_{23}\rangle_{1I} + \frac{n_1}{n_2}\frac{\langle S_2\rangle_{1R}}{L_{23}} \cdot V_2 - \frac{n_1}{n_3}\frac{\langle S_3\rangle_{1R}}{L_{23}} \cdot \langle V_3\rangle_0 \\
&\frac{d\langle i_{23}\rangle_{1I}}{dt} = -\omega_s \cdot \langle i_{23}\rangle_{1R} - \frac{R_{23}}{L_{23}} \cdot \langle i_{23}\rangle_{1I} + \frac{n_1}{n_2}\frac{\langle S_2\rangle_{1I}}{L_{23}} \cdot V_2 - \frac{n_1}{n_3}\frac{\langle S_3\rangle_{1I}}{L_{23}} \cdot \langle V_3\rangle_0
\end{aligned} \tag{9}
$$

where:

$$\langle S_2\rangle_0 = \langle S_3\rangle_0 = 0$$

$$\langle S_2\rangle_{1R} = \frac{2}{\pi} cos(D_1\pi + \varphi_2)$$

$$\langle S_2\rangle_{1I} = -\frac{2}{\pi} sin(D_1\pi + \varphi_2)$$

$$\langle S_3\rangle_{1R} = \frac{2}{\pi} cos(D_1\pi + \varphi_3)$$

$$\langle S_3\rangle_{1I} = -\tfrac{2}{\pi} sin(D_1\pi + \varphi_3)$$

$$
\begin{aligned}
\langle v_1\rangle_{1R} = \frac{1}{\pi} \cdot \Bigg(&\frac{2L_b}{(1-L_a)} \cdot \frac{n_1}{n_2} \cdot V_2 \cdot \cos(D_1\pi + \varphi_2) + \frac{2L_c}{(1-L_a)} \cdot \frac{n_1}{n_3} \cdot \langle V_3\rangle_0 \cdot \cos(D_1\pi + \varphi_3) \\
&+ \left(L_b \cdot V_2 \cdot \frac{n_1}{n_2} + L_c \cdot \langle V_3\rangle_0 \cdot \frac{n_1}{n_3}\right) \cdot \frac{\sin(\omega_s t_0)}{(1-L_a)} \Bigg)
\end{aligned}
$$

$$
\begin{aligned}
\langle v_1\rangle_{1I} = \frac{1}{\pi} \cdot \Bigg(&\frac{-2L_b}{(1-L_a)} \cdot \frac{n_1}{n_2} \cdot V_2 \cdot \sin(D_1\pi + \varphi_2) - \frac{2L_c}{(1-L_a)} \cdot \frac{n_1}{n_3} \cdot \langle V_3\rangle_0 \cdot \sin(D_1\pi + \varphi_3) \\
&+ \left(L_b \cdot V_2 \cdot \frac{n_1}{n_2} + L_c \cdot \langle V_3\rangle_0 \cdot \frac{n_1}{n_3}\right) \cdot \frac{\cos(\omega_s t_0)}{(1-L_a)} \\
&- \left(L_b \cdot V_2 \cdot \frac{n_1}{n_2} + L_c \cdot \langle V_3\rangle_0 \cdot \frac{n_1}{n_3}\right) \cdot \frac{1}{(1-L_a)} \Bigg)
\end{aligned}
$$

$$
\begin{aligned}
\langle V_{dc,1}\rangle_0 = &-2 \cdot \left(L_b \cdot V_2 \cdot \frac{n_1}{n_2} + L_c \cdot \langle V_3\rangle_0 \cdot \frac{n_1}{n_3}\right) \cdot \frac{D_1}{(1-L_a)} + 2 \cdot \left(L_b \cdot V_2 \cdot \frac{n_1}{n_2} + L_c \cdot \langle V_3\rangle_0 \cdot \frac{n_1}{n_3}\right) \cdot \frac{1}{(1-L_a)} \\
&- \frac{2L_b}{(1-L_a)} \cdot \frac{n_1}{n_2} \cdot V_2 \cdot \frac{\varphi_2}{\pi} - \frac{2L_c}{(1-L_a)} \cdot \frac{n_1}{n_3} \cdot \langle V_3\rangle_0 \cdot \frac{\varphi_3}{\pi} + \frac{4L_1}{(1-L_a) \cdot T_s} \cdot \langle i_1\rangle_0
\end{aligned}
$$

The large signal model (9) can be represented by:

$$\dot{X} = A \cdot X + B \cdot U,$$

where $X = [\langle i_1\rangle_0\ \langle V_3\rangle_0\ \langle i_{12}\rangle_{1R}\ \langle i_{12}\rangle_{1I}\ \langle i_{13}\rangle_{1R}\ \langle i_{13}\rangle_{1I}\ \langle i_{23}\rangle_{1R}\ \langle i_{23}\rangle_{1I}]^T$ and $U = [V_1\ V_2]^T$.

The control input parameters of this system are the duty cycle D_1 and the phase shifts φ_2 and φ_3. The control output parameters are $\langle i_1 \rangle_0$ and $\langle V_3 \rangle_0$. Therefore, the obtained averaged equations are non-linear. A linearization should be performed around an operating point to be able to use classical linear controllers. The small signal model of the system is obtained by introducing small perturbations to the system's variables at an operating point and using the Taylor series expansion, such that:

$$\langle x \rangle = x_{eq} + \widehat{\langle x \rangle}$$

where variables with the symbol "^" represent the small signals (perturbations around the operating point) and x_{eq} represents the value of $\langle x \rangle$ at the operating point, also called the equilibrium point.

The perturbations of the voltage sources around their average values can be neglected in this study ($\widehat{V_1} = \widehat{V_2} = 0$). This is mainly due to their slow variation compared to the fast control dynamics (ex., voltage of a PV panel, a battery system or the grid). The obtained linearized mathematical model has an order of 8.

5. Reduced-Order Model of the Hybrid-Fed TAB Converter

The reduced-order model of a system is a simplified model that can be more easily studied and employed in simulations. In addition to that, it makes the design of the system controllers a lot simpler [25]. Consequently, it would be possible to recalculate the system's controllers in real time when a change in the operating point occurs. However, the main drawback of this order reduction is the decreased precision of the mathematical model.

Reduced-order averaged modeling relies on splitting the system's dynamics in the frequency domain into two parts: the low-frequency dynamics (slow variables) and the high-frequency dynamics (fast variables) [25]. After that, only the dominant dynamics are considered for the study of the system's behavior.

For the hybrid-fed TAB converter, the DC variables can be considered as slow variables and the AC variables as fast variables. In this case, the slow variables represent the input/output parameters of the system, whereas the fast variables represent the internal functioning of the converter. Since the control of this TAB converter aims to regulate the slow input/output parameters, the dominant low-frequency dynamics are preserved and the fast dynamics are ignored in the reduced-order model. The two subsystems can therefore be represented as follows:

- The slow-dynamics subsystem which will be indexed by "s",
- The fast-dynamics subsystem which will be indexed by "f".

The state vector X of the full-order system (9) will then be split into two parts:

$$X = \begin{bmatrix} X_s & X_f \end{bmatrix}^T$$

where: $X_s = [\langle i_1 \rangle_0 \quad \langle V_3 \rangle_0]^T$ and $X_f = [\langle i_{12} \rangle_{1R} \quad \langle i_{12} \rangle_{1I} \quad \langle i_{13} \rangle_{1R} \quad \langle i_{13} \rangle_{1I} \quad \langle i_{23} \rangle_{1R} \quad \langle i_{23} \rangle_{1I}]^T$.

Therefore, system (9) becomes:

$$\dot{X} = A \cdot X + B \cdot U \rightarrow \begin{cases} \dot{X}_s = A_{ss} \cdot X_s + A_{sf} \cdot X_f + B_s \cdot U \\ \dot{X}_f = A_{fs} \cdot X_s + A_{ff} \cdot X_f + B_f \cdot U \end{cases}$$

Matrices A_{ss}, A_{sf}, A_{fs}, A_{ff}, B_s and B_f are obtained through a proper rearrangement of matrices A and B. To obtain the reduced-order model, we start by solving the fast dynamics subsystem at a chosen operating (equilibrium) point ($\dot{X}_{f,eq} = 0$), by considering the slow variables constant and equal to their average values ($X_s = X_{s,eq}$, so $\langle i_1 \rangle_0 = I_{1,eq}$ and $\langle V_3 \rangle_0 = V_{3,eq}$). The average response $X_{f,eq}$ of the fast subsystem is obtained from this step. After that, in the slow subsystem, the fast variables will be replaced by their average response ($X_f = X_{f,eq}$) calculated in the previous step. Then, the slow subsystem is linearized around the chosen operating point while ignoring the dynamics of the fast

variables. This will give us the linearized reduced-order model of the converter, which is:

$$\frac{d\langle\hat{i}_1\rangle_0}{dt} = \left(-\frac{R_f}{L_f} - \frac{4L_1}{L_f\cdot(1-L_a)\cdot T_s}\right)\cdot\langle\hat{i}_1\rangle_0 + \frac{2L_c}{L_f\cdot(1-L_a)}\cdot\frac{n_1}{n_3}\left(D_{1,eq} - 1 + \frac{\varphi_{3,eq}}{\pi}\right)\cdot\langle\hat{V}_3\rangle_0 + \left(\frac{2L_b}{L_f\cdot(1-L_a)}\cdot\frac{n_1}{n_2}\cdot V_2 + \frac{2L_c}{L_f\cdot(1-L_a)}\cdot\frac{n_1}{n_3}\cdot V_{3,\mathrm{eq}}\right)\cdot\hat{D}_1 + \frac{2L_b}{L_f\cdot(1-L_a)}\cdot\frac{n_1}{n_2}\cdot V_2 \cdot\frac{\hat{\varphi}_2}{\pi} + \frac{2L_c}{L_f\cdot(1-L_a)}\cdot\frac{n_1}{n_3}\cdot V_{3,\mathrm{eq}}\cdot\frac{\hat{\varphi}_3}{\pi}$$

$$\frac{d\langle\hat{V}_3\rangle_0}{dt} = -\frac{\langle\hat{V}_3\rangle_0}{C_3R_{L3}} - \frac{4}{C_3}\cdot\frac{n_1}{n_3}\cdot\left[I_{13,R,eq}\cdot\sin\left(D_{1,eq}\cdot\pi+\varphi_{3,eq}\right) + I_{13,I,eq}\cdot\cos\left(D_{1,eq}\cdot\pi+\varphi_{3,eq}\right) + I_{23,R,eq}\cdot\sin\left(D_{1,eq}\cdot\pi+\varphi_{3,eq}\right) + I_{23,I,eq}\cdot\cos\left(D_{1,eq}\cdot\pi+\varphi_{3,eq}\right)\right]\cdot\hat{D}_1 - \frac{4}{\pi C_3}\cdot\frac{n_1}{n_3}\cdot\left[I_{13,R,eq}\cdot\sin\left(D_{1,eq}\cdot\pi+\varphi_{3,eq}\right) + I_{13,I,eq}\cdot\cos\left(D_{1,eq}\cdot\pi+\varphi_{3,eq}\right) + I_{23,R,eq}\cdot\sin\left(D_{1,eq}\cdot\pi+\varphi_{3,eq}\right) + I_{23,I,eq}\cdot\cos\left(D_{1,eq}\cdot\pi+\varphi_{3,eq}\right)\right]\cdot\hat{\varphi}_3 \quad (10)$$

As can be noticed, the order of the system's mathematical model has been reduced from eight to two by using the reduced-order modeling method. This will make the study of the dynamical behavior and the control design of the TAB converter simpler.

The Laplace transform of the obtained linearized reduced-order model (10) will lead to the following reduced transfer functions linking the input current I_1 of port 1 to the duty cycle D_1 on the one hand, and the output DC voltage V_3 of port 3 to the phase shift φ_3 on the other hand:

$$G_{i1_r}(s) = \left.\frac{I_1(s)}{D_1(s)}\right|_{\substack{\hat{\varphi}_2=0\\ \hat{\varphi}_3=0}} = \frac{a\cdot s+b}{(s+c)(s+d)} \quad (11)$$

$$G_{v3_r}(s) = \left.\frac{V_3(s)}{\varphi_3(s)}\right|_{\substack{\hat{\varphi}_2=0\\ \hat{D}_1=0}} = \frac{e}{(s+d)} \quad (12)$$

With:

$$a = \frac{2L_b}{L_f\cdot(1-L_a)}\cdot\frac{n_1}{n_2}\cdot V_2 + \frac{2L_c}{L_f\cdot(1-L_a)}\cdot\frac{n_1}{n_3}\cdot V_{3,\mathrm{eq}}$$

$$b = \frac{a}{C_3R_{L3}} - \frac{8}{C_3}\cdot\frac{L_c}{L_f\cdot(1-L_a)}\cdot\left(\frac{n_1}{n_3}\right)^2\cdot\left(D_{1,eq}-1+\frac{\varphi_{3,eq}}{\pi}\right)\cdot\left(I_{13,R,eq}\cdot\sin\left(D_{1,eq}\cdot\pi+\varphi_{3,eq}\right) + I_{13,I,eq}\cdot\cos\left(D_{1,eq}\cdot\pi+\varphi_{3,eq}\right) + I_{23,R,eq}\cdot\sin\left(D_{1,eq}\cdot\pi+\varphi_{3,eq}\right) + I_{23,I,eq}\cdot\cos\left(D_{1,eq}\cdot\pi+\varphi_{3,eq}\right)\right)$$

$$c = \frac{R_f}{L_f} + \frac{4L_1}{L_f\cdot(1-L_a)\cdot T_s}$$

$$d = \frac{1}{C_3R_{L3}}$$

$$e = \frac{4}{\pi C_3}\cdot\frac{n_1}{n_3}\cdot\left(I_{13,R,eq}\cdot\sin\left(D_{1,eq}\cdot\pi+\varphi_{3,eq}\right) + I_{13,I,eq}\cdot\cos\left(D_{1,eq}\cdot\pi+\varphi_{3,eq}\right) + I_{23,R,eq}\cdot\sin\left(D_{1,eq}\cdot\pi+\varphi_{3,eq}\right) + I_{23,I,eq}\cdot\cos\left(D_{1,eq}\cdot\pi+\varphi_{3,eq}\right)\right)$$

Figure 5 compares the bode plots of the full order transfer functions (G_{v3} and G_{i1}) calculated from the linearization of system (9) to the reduced order ones (G_{v3_r} and G_{i1_r}) expressed in Equations (11) and (12). As we can notice, the full order and the reduced

order responses of each one of these two transfer functions are similar at low frequencies (below the switching frequency where the resonance occurs). This proves that the reduced-order model represents the system's slow dynamics appropriately and as expected.

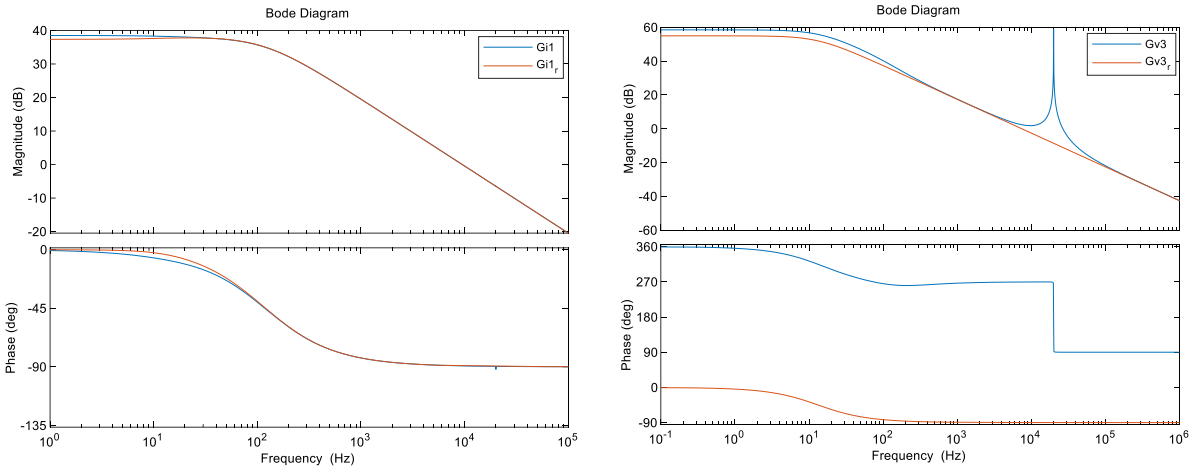

(**a**) (**b**)

Figure 5. Comparison of the bode plots of the full-order model and the reduced-order model of the hybrid-fed TAB converter: (**a**) input current I_1 of port 1; (**b**) output voltage V_3 of port 3.

Furthermore, the transfer function G_{i1_r} can also be reduced by ignoring the dynamics of voltage V_3, considering that it does not vary a lot around its nominal value. The new reduced transfer function will therefore be a first order transfer function having the following expression:

$$G_{i1_{r2}}(s) = \frac{I_1(s)}{D_1(s)}\bigg|_{\substack{\tilde{\varphi}_2=0 \\ \tilde{\varphi}_3=0 \\ \tilde{V}_3=0}} = \frac{a}{(s+c)} \tag{13}$$

Figure 6 compares the bode plots of the full-order transfer function G_{i1} calculated from the linearization of system (9) and the two reduced-order transfer functions of Equations (11) and (13) (G_{i1_r} and $G_{i1_{r2}}$). We can notice that the responses of these three plots are similar at low frequencies, proving that the current control's slow dynamics can also be represented by $G_{i1_{r2}}$, further simplifying the system's order.

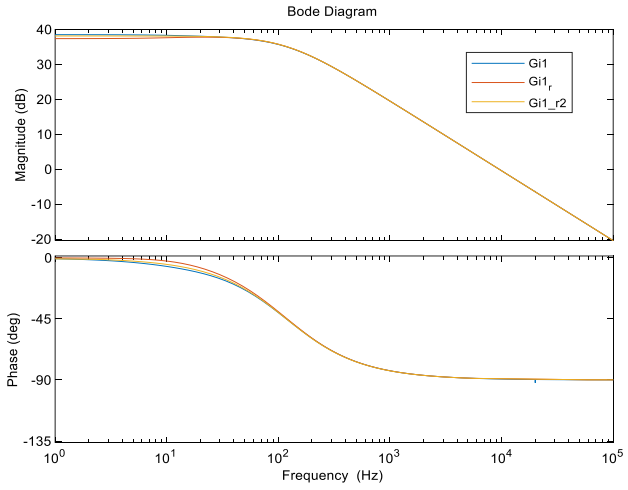

Figure 6. Comparison of the bode plots of the full-order model and the two reduced-order models of the DC current control of port 1.

We deduce from Figures 5 and 6 that the first order transfer functions $G_{i1_{r2}}$ and G_{v3_r} can be used to study and control the DC current of port 1 and the DC voltage of port 3 of this TAB converter, as their responses are sufficiently close to the full-order model's results.

The order of the reduced transfer functions G_{v3_r} and $G_{i1_{r2}}$ is independent of the number of ports of the TAB converter. Therefore, this developed reduced-order model of the hybrid-fed TAB converter can be generalized to a hybrid-fed MAB converter having n-ports, one of which is current-fed while the $(n-1)$ others are voltage-fed ports. These two reduced-order functions will then still be first order functions regardless of the number of ports of the MAB converter, such that the voltages of the voltage-fed ports do not vary a lot around their average values for a certain operating point.

The reduced-order models developed in this section will be used in the following sections to study the behavior of this hybrid-fed TAB converter and to design its closed-loop controllers.

6. Control Strategy

Two parameters should be controlled in this system (control output parameters): the DC input current I_1 of port 1 and the DC output voltage V_3 of port 3. However, the control input parameters are three: D_1, φ_2 and φ_3. Therefore, at a chosen operating point, an infinity of combinations of the values of $D_{1,eq}$, $\varphi_{2,eq}$ and $\varphi_{3,eq}$ can give us the same desired values of $I_{1,eq}$ and $V_{3,eq}$, as long as the conditions of expressions (4) to (6) are respected. Additionally, from system (9), we can notice that each control output ($I_{1,eq}$ and $V_{3,eq}$) depends on all the control inputs ($D_{1,eq}$, $\varphi_{2,eq}$ and $\varphi_{3,eq}$) of the system. This proves that the studied TAB structure is coupled and a change in one of the control variables will affect all the ports.

One way to control this hybrid-fed TAB converter is by making $D_{1,\mathrm{eq}}$ equal to its minimum allowed value expressed in (4) with an added safety margin ϵ at each operating point ($D_{1,eq} = D_{1,min} + \epsilon$). The corresponding values of $\varphi_{2,eq}$ and $\varphi_{3,eq}$ are then calculated from the full-order model expressed in system (9) at the chosen operating point. The calculated values of the three control parameters are then feedforwarded to the system. Adding a feedforward to the control of the TAB converter will lead to the decoupling of its ports control, as explained in [8]. Then, from (5) and (6), we get the minimum allowed values of φ_2 and φ_3.

The approximations that were performed in the developed mathematical model will lead to a steady state error if only an open loop (feedforward) control is applied. A PI controller is therefore used for each control loop in order to delete this error (Figure 7). These controllers are calculated based on the reduced-order model that was developed in the previous section. Adaptable saturation blocks are finally added to the control system in order to ensure that conditions (4) to (6) are always satisfied. These blocks are also shown in Figure 7, where the maximum and minimum allowed values of D_1 and φ_3 are dynamically calculated.

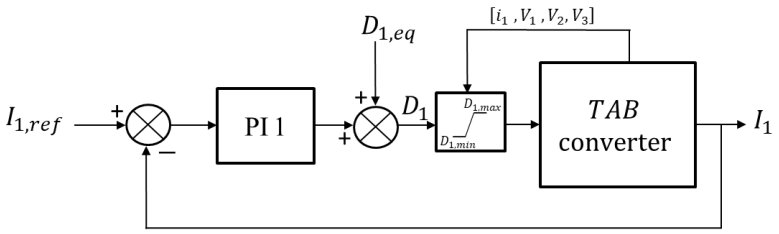

(**a**)

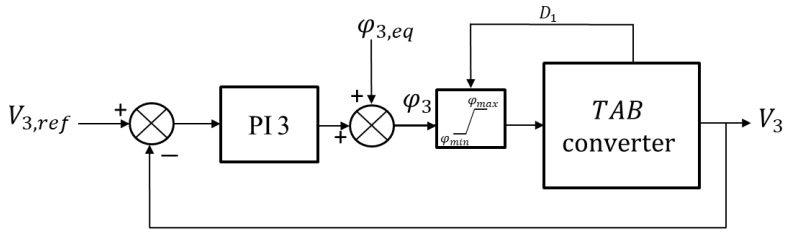

(**b**)

Figure 7. Control block diagrams of the hybrid-fed TAB converter: (**a**) DC current control of port 1; (**b**) DC voltage control of port 3.

In Figure 7, $D_{1,\max}$ is the maximum allowed value for D_1 and it is equal to one. $\varphi_{\max}$ is the maximum allowed value for φ_2 and φ_3 and it is calculated as follows:

$$t_5 \le T_s \; and \; t_6 \le T_s \rightarrow \varphi_{\max} = \pi \cdot \left(\frac{3}{2} - D_1\right)$$

The controllers PI1 and PI3 have the following expressions, respectively:

$$C_1(s) = \frac{K_{p1} \cdot (T_{i1} \cdot s + 1)}{T_{i1} \cdot s} \; ; \; C_3(s) = \frac{K_{p3} \cdot (T_{i3} \cdot s + 1)}{T_{i3} \cdot s}$$

6.1. Input DC Current Control of Port 1

The transfer function $G_{i1_{r2}}$ of Equation (13) is used to calculate the parameters of the controller PI1 for the input DC current control of port 1. It is a first order transfer function.

We choose $T_{i1} = \frac{1}{c}$. The closed loop transfer function will therefore become:

$$CLTF_1(s) = \frac{C_1(s)G_{i1}(s)}{1 + C_1(s)G_{i1}(s)} = \frac{K_{p1} \cdot a}{s + K_{p1} \cdot a} = \frac{1}{\tau_1 \cdot s + 1}$$

With $\tau_1 = \frac{1}{K_{p1} \cdot a}$ the time constant of the closed loop system.

Considering that the time response value of this closed loop transfer function to reach 95% of the desired current reference is $t_{r1,95\%} = 3.\tau_1$, the gain K_{p1} is chosen for a desired value of $t_{r1,95\%}$, such that:

$$K_{p1} = \frac{3}{a \cdot t_{r1,95\%}} \tag{14}$$

6.2. Output DC Voltage Control of Port 3

The transfer function G_{v3_r} of Equation (12) is used to calculate the parameters of controller PI3 for the output DC voltage control of port 3. It is a first order transfer function.

We choose $T_{i3} = \frac{1}{d}$. The closed loop transfer function will therefore be:

$$CLTF_3(s) = \frac{C_3(s)G_{v3}(s)}{1 + C_3(s)G_{v3}(s)} = \frac{K_{p3} \cdot e}{s + K_{p3} \cdot e} = \frac{1}{\tau_3 \cdot s + 1}$$

With $\tau_3 = \frac{1}{K_{p3} \cdot e}$ the time constant of the closed loop system.

Considering that the time response value of this closed loop transfer function to reach 95% of the desired voltage reference is $t_{r3,95\%} = 3.\tau_3$, the gain K_{p3} is chosen for a desired value of $t_{r3,95\%}$, such that:

$$K_{p3} = \frac{3}{e \cdot t_{r3,95\%}} \tag{15}$$

7. Simulated Results and Discussion

Figure 8 shows the simulation results of the closed loop control of current I_1 of this system, when a setpoint change is applied. Table 1 presents the parameter values used for the different ports of the simulated TAB converter. The time response that was chosen to reach the parameter values of controller PI1 from Equation (14) is $t_{r1,95\%} = 3$ ms. We can see from Figure 8 that the closed loop time response of the simulated switched model is equal to its chosen value (3 ms), which validates the developed mathematical model and control strategy. The ripple of this current depends on the value of the inductance L_f, which is chosen according to design requirements. Therefore, according to the application in which this TAB converter is expected to be integrated, the value of L_f can be adjusted (increased to decrease the ripple).

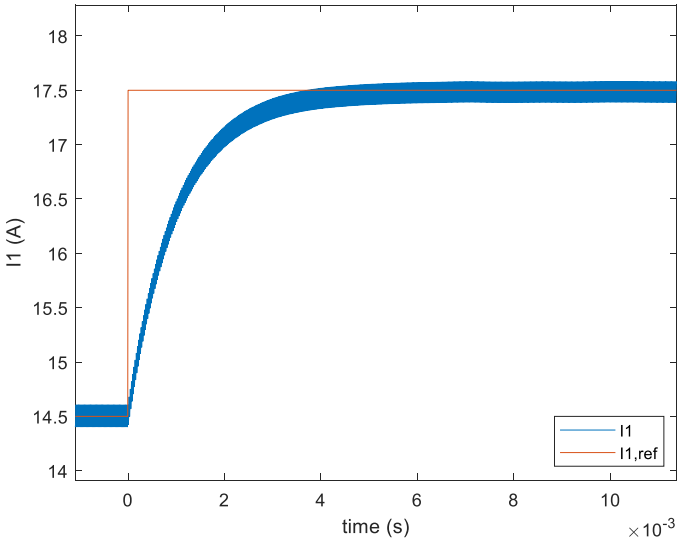

Figure 8. Simulation results of the current closed-loop control developed for port 1 of the hybrid-fed TAB converter.

Table 1. Parameter values of the simulated coupled hybrid-fed TAB converter.

Parameter Symbol	Parameter Value
V_1	200 V
V_2	400 V
f_s	20 KHz
L_f	0.016 H
R_f	10 mΩ
L_1	83 µH
R_1	10 mΩ
L_2	83 µH
R_2	10 mΩ
L_3	230 µH
R_3	10 mΩ
C_3	100 µH
R_{c3}	1 mΩ
L_m	8.3 mH
n_1	100 turns
n_2	83 turns
n_3	124 turns
$P_{3,nominal}$	3 KW (received)
$P_{1,nominal}$	3.5 KW (delivered)

P_{max} (between 2 ports)	4 KW
R_{L3}	120 Ω

Figure 9 shows the simulation results of the closed loop control of voltage V_3 of this system, when a setpoint change is applied. The time response that was chosen to get the parameter values of controller PI3 from Equation (15) is $t_{r3,95\%} = 10$ ms. We can see from Figure 9 that the closed-loop time response of the simulated switched model is equal to its chosen value (10 ms), which validates the developed mathematical model and controller.

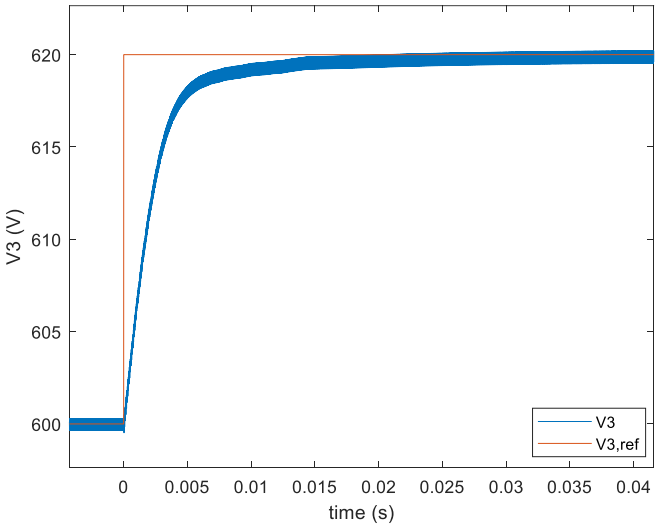

Figure 9. Simulation results of the voltage closed-loop control developed for port 3 of the hybrid-fed TAB converter.

The minor mismatch between the chosen characteristics for the calculation of the controllers' parameters and the characteristics of the simulated responses is due to the simplifying hypotheses that were conducted while developing the mathematical model, especially the first harmonic approximation of the AC signals and the model order reduction. In order to further improve the accuracy of the proposed model, a higher harmonic order can be considered. However, this will increase the complexity of the model. The proposed model offers a fair compromise between accuracy and complexity.

Figure 10 shows the waveforms of the control parameters of the hybrid-fed TAB converter when the setpoint of current i_1 is changed ($t_{r1,95\%} = 20$ ms).

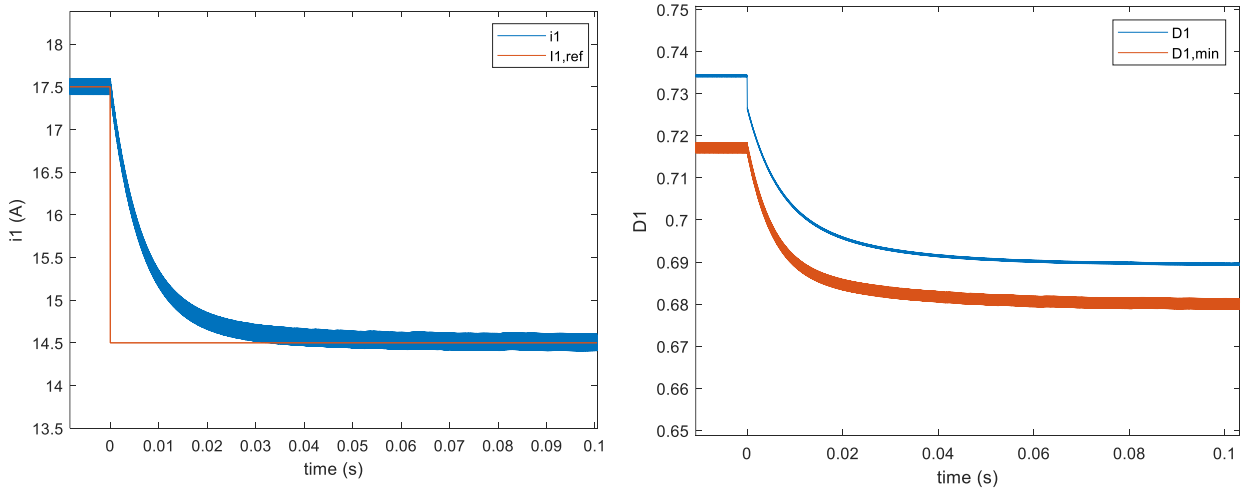

(**a**) (**b**)

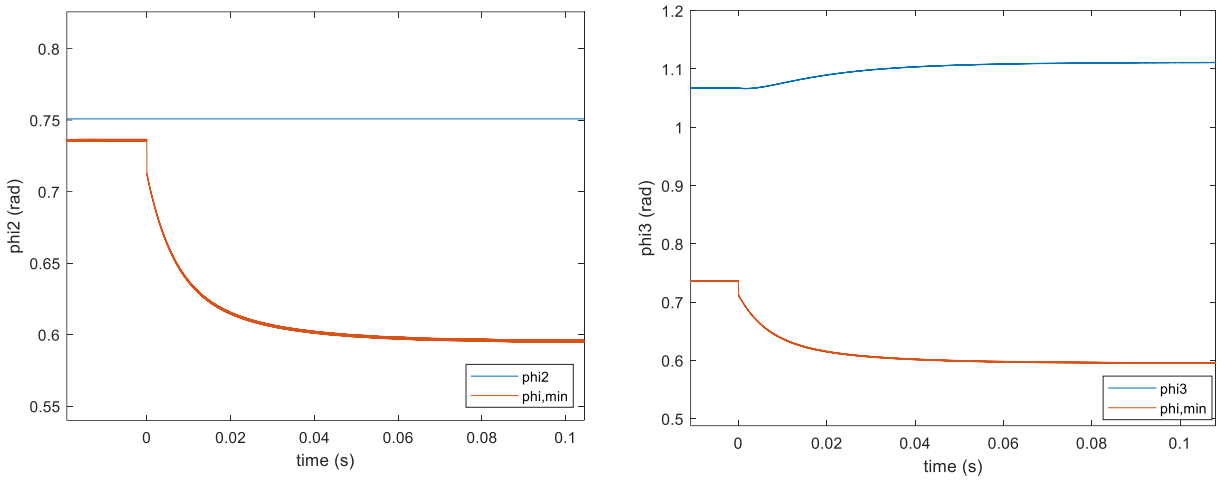

(**c**) (**d**)

Figure 10. Waveforms of the hybrid-fed TAB converter: (**a**) input current i_1 of port 1; (**b**) duty cycle D_1 of command signal of port 1; (**c**) phase shift φ_2 of command signal of port 2; (**d**) phase shift φ_3 of command signal of port 3.

For the results shown in Figure 10, saturation blocks were added to the control parameters D_1, φ_2 and φ_3, as shown in Figure 7, to avoid the non-compliance of conditions (4) to (6). A safety margin of $\epsilon = 0.01$ for the control of D_1 was also taken into consideration ($D_{1,eq} = D_{1,min} + \epsilon$). This value was chosen arbitrarily in this study. As we can notice, current i_1 follows its reference value with the expected response characteristics, while the values of all the control input parameters stay within their allowed intervals.

Figure 11 shows the AC voltages at the three transformer windings and the AC current of port 1. No overvoltages have occurred at the current port. Additionally, the waveforms of i_{L1}, v_2 and v_3 shown in Figure 11 match their theoretical waveforms drawn in Figure 2 and the waveform of v_1 matches its developed expressions in Section 2.2. This validates the developed model and the proposed control strategy.

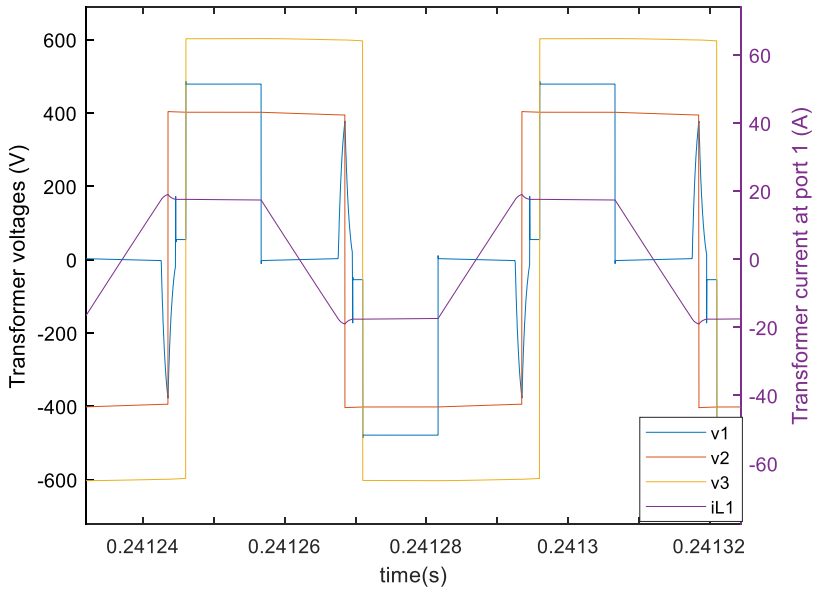

Figure 11. Waveforms of the AC voltages of the three ports and the AC current of port 1 with saturation blocks on the three control parameters and a safety margin $\epsilon = 0.01$ on the command of D_1.

8. Conclusions

A hybrid-fed MAB converter is an interesting topology for many applications such as PV panels and battery storage systems. This is mainly due to their soft-switching performances on the whole operation range. However, current-fed ports add operational restrictions to the system, which leads to questioning the feasibility of the closed-loop control of such topologies.

In this paper, the mathematical modelling and control of a hybrid-fed TAB converter were developed. The working concept of this topology was explained and so were the control conditions that should be respected for a safe functioning without overvoltages and with soft switching. After that, a generalized average model and a reduced-order model of this system were elaborated and compared. A control strategy was proposed based on the developed models and control conditions. The full-order model was used for the calculation of the feedforwarded control parameters when a setpoint change occurs. This will set the system in a state very close to its desired operating point. The error is then cancelled by PI controllers. The reduced-order model is used to calculate these PI controllers and to simplify the dynamic behavior study of the system. Adaptable saturation blocks were employed in the control of this TAB converter in order to ensure that the operating conditions are always satisfied, especially when moving from an operating point to another. The mathematical models and the developed control technique were tested and validated using Matlab/Simulink.

The obtained simulation results show the closed-loop response of the input current control of the current-fed port and the output voltage control of one of the voltage-fed ports. Controlling these two variables will allow control of the power flows between the different ports of the proposed three-ported topology. The expected characteristics chosen while calculating the PI controllers' parameters were attained in these responses and no overvoltages have occurred at the current-fed port. This answers the main question of this research, proving that the closed-loop control of the proposed topology is possible.

The modelling and control strategy presented in this paper can be generalized for a hybrid-fed MAB converter with any number of ports, one of which is current-fed. However, the more voltage ports are added, the more control restrictions should be respected and the more complex the system control becomes.

In future works, for the hybrid-fed TAB converter topology presented in this paper, the three control input parameters (D_1, φ_2 and φ_3) could be chosen in a different way in order to improve the system's efficiency by reducing its transformer's RMS currents, for example (instead of choosing the combination of control input parameters where $D_{1,eq} = D_{1,min} + \epsilon$). Additionally, it would be interesting to elaborate an emergency stop strategy for these types of converters.

Author Contributions: Conceptualization, R.T. and D.F.; Methodology, R.T. and D.F.; Supervision, D.F., S.L., S.C., X.M. and Y.L.; Validation, R.T., D.F., S.L., S.C., X.M. and Y.L.; Writing—original draft, R.T.; Writing—review and editing, D.F., S.L., S.C., X.M. and Y.L. All authors have read and agreed to the published version of the manuscript.

Funding: This research received no external funding.

Data Availability Statement: All the reported data are included in the manuscript.

Conflicts of Interest: The authors declare no conflict of interest.

References

1. Adil, A.M.; Ko, Y. Socio-technical evolution of Decentralized Energy Systems: A critical review and implications for urban planning and policy. *Renew. Sustain. Energy Rev.* **2016**, *57*, 1025–1037. https://doi.org/10.1016/j.rser.2015.12.079.
2. Werth, A.; Kitamura, N.; Tanaka, K. Conceptual Study for Open Energy Systems: Distributed Energy Network Using Interconnected DC Nanogrids. *IEEE Trans. Smart Grid* **2015**, *6*, 1621–1630. https://doi.org/10.1109/TSG.2015.2408603.
3. Mohammadi, M.; Noorollahi, Y.; Mohammadi-ivatloo, B.; Yousefi, H. Energy hub: From a model to a concept—A review. *Renew. Sustain. Energy Rev.* **2017**, *80*, 1512–1527. https://doi.org/10.1016/j.rser.2017.07.030.

4. Galeshi, S. "Cluster" Converters Based on Multi-Port Active-Bridge: Application to Smartgrids, Ph.D. Thesis, Université Grenoble Alpes, Saint-Martin-d'Hères, France, 2021.
5. Blanc, M.; Lembeye, Y.; Ferrieux, J.-P. Dual Active Bridge (DAB) pour la conversion continu-continu. *Tech. l'Ingénieur Électronique* **2019**, *E3975 V1*, 1–23. https://doi.org/10.51257/a-v1-e3975.
6. Chen, Y.; Wang, P.; Li, H.; Chen, M. Power Flow Control in Multi-Active-Bridge Converters: Theories and Applications. In Proceedings of the 2019 IEEE Applied Power Electronics Conference and Exposition (APEC), Anaheim, CA, USA, 17–21 March 2019; pp. 1500–1507. https://doi.org/10.1109/APEC.2019.8722122
7. Galeshi, S.; Frey, D.; Lembeye, Y. Efficient and scalable power control in multi-port active-bridge converters. In Proceedings of the 2020 22nd European Conference on Power Electronics and Applications (EPE'20 ECCE Europe), Lyon, France, 7–11 September 2020; pp. P.1–P.9. https://doi.org/10.23919/EPE20ECCEEurope43536.2020.9215905.
8. Zhao, C.; Round, S.D.; Kolar, J.W. An Isolated Three-Port Bidirectional DC-DC Converter with Decoupled Power Flow Management. *IEEE Trans. Power Electron.* **2008**, *23*, 2443–2453. https://doi.org/10.1109/TPEL.2008.2002056.
9. Tao, H.; Kotsopoulos, A.; Duarte, J.L.; Hendrix, M.A.M. A Soft-Switched Three-Port Bidirectional Converter for Fuel Cell and Supercapacitor Applications. In Proceedings of the IEEE 36th Conference on Power Electronics Specialists, Dresden, Germany, 16 June 2005; pp. 2487–2493. https://doi.org/10.1109/PESC.2005.1581982.
10. Dey, S.; Mallik, A.; Akturk, A. Investigation of ZVS Criteria and Optimization of Switching Loss in a Triple Active Bridge Converter Using Penta-Phase-Shift Modulation. *IEEE J. Emerg. Sel. Top. Power Electron.* **2022**, *10*, 7014–7028. https://doi.org/10.1109/JESTPE.2022.3191987.
11. Purgat, P.; Bandyopadhyay, S.; Qin, Z.; Bauer, P. Zero Voltage Switching Criteria of Triple Active Bridge Converter. *IEEE Trans. Power Electron.* **2021**, *36*, 5425–5439. https://doi.org/10.1109/TPEL.2020.3027785.
12. Hebala, O.M.; Aboushady, A.A.; Ahmed, K.H.; Abdelsalam, I. Generalized Active Power Flow Controller for Multiactive Bridge DC–DC Converters with Minimum-Current-Point-Tracking Algorithm. *IEEE Trans. Ind. Electron.* **2022**, *69*, 3764–3775. https://doi.org/10.1109/TIE.2021.3071681.
13. Blinov, A.; Vinnikov, D.; Ivakhno, V. Full soft-switching high step-up DC-DC converter for photovoltaic applications. In Proceedings of the 2014 16th European Conference on Power Electronics and Applications, Lappeenranta, Finland, 26–28 August 2014; pp. 1–7. https://doi.org/10.1109/EPE.2014.6911013.
14. Guo, Z.; Sun, K.; Wu, T.-F.; Li, C. An Improved Modulation Scheme of Current-Fed Bidirectional DC–DC Converters for Loss Reduction. *IEEE Trans. Power Electron.* **2018**, *33*, 4441–4457. https://doi.org/10.1109/TPEL.2017.2719722.
15. Chub, A.; Rabkowski, J.; Blinov, A.; Vinnikov, D. Study on power losses of the full soft-switching current-fed DC/DC converter with Si and GaN devices. In Proceedings of the IECON 2015-41st Annual Conference of the IEEE Industrial Electronics Society, Yokohama, Japan, 9–12 November 2015; pp. 13–18. https://doi.org/10.1109/IECON.2015.7392957.
16. Chub, A.; Kosenko, R.; Blinov, A. Zero-voltage switching galvanically isolated current-fed full-bridge DC-DC converter. In Proceedings of the 2016 10th International Conference on Compatibility, Power Electronics and Power Engineering (CPE-POWERENG), Bydgoszcz, Poland, 29 June–1 July 2016; pp. 455–459. https://doi.org/10.1109/CPE.2016.7544231.
17. Kurm, S.; Agarwal, V. Current Fed Dual Active Bridge based Multi-Port DC/AC Converter for Standalone Solar PV fed Systems with Battery Backup. In Proceedings of the 2020 IEEE International Conference on Power Electronics, Drives and Energy Systems (PEDES), Jaipur, India, 16–19 December 2020; pp. 1–6. https://doi.org/10.1109/PEDES49360.2020.9379447.
18. Yaow-Ming Chen; Yuan-Chuan Liu; Feng-Yu Wu Multi-input DC/DC converter based on the multiwinding transformer for renewable energy applications. *IEEE Trans. Ind. Applicat.* **2002**, *38*, 1096–1104. https://doi.org/10.1109/TIA.2002.800776.
19. Rathore, V.; Rajashekara, K.; Ray, A.; Rodriguez, L.A.G.; Mueller, J. A Current-fed High Gain Multilevel DC-DC Converter for BESS Grid Integration Applications. In Proceedings of the 2021 IEEE Applied Power Electronics Conference and Exposition (APEC), Phoenix, AZ, USA, 14–17 June 2021; pp. 1964–1970. https://doi.org/10.1109/APEC42165.2021.9487339.
20. Tarraf, R.; Morel, B.; Frey, D.; Leirens, S.; Carcouet, S.; Maynard, X.; Lembeye, Y. Modeling and Control of a Decoupled Hybrid-Fed Multi-Active Bridge (MAB) Converter. In Proceedings of the PCIM Europe 2023, International Exhibition and Conference for Power Electronics, Intelligent Motion, Renewable Energy and Energy Management, Nuremberg, Germany, 9–11 May 2023, pp. 1–9. https://doi.org/10.30420/566091242.
21. Bandyopadhyay, S.; Purgat, P.; Qin, Z.; Bauer, P. A Multiactive Bridge Converter with Inherently Decoupled Power Flows. *IEEE Trans. Power Electron.* **2021**, *36*, 2231–2245. https://doi.org/10.1109/TPEL.2020.3006266.
22. Purgat, P.; Bandyopadhyay, S.; Qin, Z.; Bauer, P. Continuous Full Order Model of Triple Active Bridge Converter. In Proceedings of the 2019 21st European Conference on Power Electronics and Applications (EPE '19 ECCE Europe), Genova, Italy, 3–5 September 2019; pp. P.1–P.9. https://doi.org/10.23919/EPE.2019.8914897.
23. Foch, H.; Chéron, Y.; Arches, R.; Escaut, B.; Marty, P.; Metz, M. Commutateurs de courant. *Tech. l'Ingénieur Convers. l'Energie Electrique* **1993**, *D3171 V1*, 1–2. https://doi.org/10.51257/a-v1-d3171.

24. Hengsi, Q.; Kimball, J.W. Generalized Average Modeling of Dual Active Bridge DC–DC Converter. *IEEE Trans. Power Electron.* **2012**, *27*, 2078–2084. https://doi.org/10.1109/TPEL.2011.2165734.
25. Bacha, S.; Munteanu, I.; Bratcu, A.I. Power Electronic Converters Modeling and Control. In *Advanced Textbooks in Control and Signal Processing*; Springer: London, UK, 2014; ISBN 978-1-4471-5477-8.